EWS splicing regulation contributes to balancing *Foxp1* isoforms required for neuronal differentiation

Veronica Verdile[1,2], Francesca Svetoni[2], Piergiorgio La Rosa[2], Gabriele Ferrante[2], Eleonora Cesari[3], Claudio Sette [3,4] and Maria Paola Paronetto [1,2,*]

[1]Department of Movement, Human and Health Sciences, University of Rome "Foro Italico", Piazza Lauro de Bosis 6, 00135 Rome, Italy, [2]Laboratory of Molecular and Cellular Neurobiology, Fondazione Santa Lucia, Via del Fosso di Fiorano, 64, 00143 Rome, Italy, [3]GSTEP-Organoids Core Facility, IRCCS Fondazione Policlinico Agostino Gemelli, 00168 Rome, Italy and [4]Department of Neuroscience, Section of Human Anatomy, Catholic University of the Sacred Hearth, 00168 Rome, Italy

ABSTRACT

Alternative splicing is a key regulatory process underlying the amplification of genomic information and the expansion of proteomic diversity, particularly in brain. Here, we identify the Ewing sarcoma protein (EWS) as a new player of alternative splicing regulation during neuronal differentiation. Knockdown of EWS in neuronal progenitor cells leads to premature differentiation. Transcriptome profiling of EWS-depleted cells revealed global changes in splicing regulation. Bioinformatic analyses and biochemical experiments demonstrated that EWS regulates alternative exons in a position-dependent fashion. Notably, several EWS-regulated splicing events are physiologically modulated during neuronal differentiation and EWS depletion in neuronal precursors anticipates the splicing-pattern of mature neurons. Among other targets, we found that EWS controls the alternative splicing of the forkhead family transcription factor FOXP1, a pivotal transcriptional regulator of neuronal differentiation, possibly contributing to the switch of gene expression underlying the neuronal differentiation program.

INTRODUCTION

The Ewing Sarcoma protein (EWS) is a DNA/RNA binding protein of the FET family, which also comprises FUS (*Fused in Liposarcoma*) and TAF15 (*TATA-box binding protein Associated Factor 15*) (1). FET proteins are characterized by a serine–tyrosine–glycine–glutamine (SYGQ)-rich domain at the N-terminus, acting as a transcriptional activation domain, a central RNA recognition motif (RRM), and three glycine–arginine (RGG) rich regions at the C-terminus, which affect the RNA binding affinity (2,3). These proteins regulate multiple steps of RNA metabolism and are involved in several biological and pathological processes (1–3).

The *EWSR1* gene is famous for its involvement in the characteristic chromosomal translocations leading to Ewing Sarcoma malignancies, tumors of bone and soft tissues that mainly affect children and adolescents (4,5). In most cases, the chromosomal translocations generate in-frame fusions between the amino terminus of EWS and the carboxyl terminus of various ETS transcription factors, generating an oncogenic transcription factor that drives neoplastic transformation (4,6). More recently, *EWSR1* mutations have been identified in Amyotrophic Lateral Sclerosis (ALS) patients (7). The ALS-associated mutations involve the RGG domain and the nuclear localization signal (NLS) of EWS, leading to mislocalization of the protein from the nucleus to the cytoplasm and impairing its nuclear activity (7,8).

Knockout of the *Ewsr1* gene in the mouse leads to high (~90%) postnatal lethality prior to weaning and the few surviving *Ewsr1−/−* mice are infertile due to impaired germ cell differentiation in both sexes (9). Loss of *Ewsr1* function also leads to premature symptoms of aging, and defects in B lymphocytes (9,10) and dermal development (11). More recently, *Ewsr1−/−* mice were reported to display defects in neuronal morphology and impairment of the dopaminergic signaling pathway, followed by motor dysfunction (12). However, the specific role played by EWS in the brain has not been investigated yet. Notably, EWS expression is fine-tuned at post-transcriptional level by miR-141 during mouse brain development and neuronal differentiation in culture (13). Moreover, a brain-specific isoform of EWS including a 18 bp-exon is expressed from embryonic day 11.5 (E11.5) to birth, paralleling the decrease of the main isoform (14), whereas expression of both isoforms declines steadily after birth (14). While these observations suggest that EWS function needs to be modulated during brain

---

development, the specific role played by this protein during neuronal differentiation is currently unknown. One of the best characterized functions of EWS is the regulation of alternative splicing (AS). In particular, EWS was shown to directly interact with the RNA Polymerase II ([2](#)) and the U1 snRNP component of the spliceosome ([15–18](#)) and to modulate selected splicing events in human cells. However, whether or not EWS modulates the transcriptome of neurons though splicing regulation during development has not been investigated to date.

AS is combinatorial process through which exons are differentially assorted in the mature transcript ([19–21](#)), thus generating multiple transcript variants from each gene and amplifying the genome and proteome complexity of organisms ([22–25](#)). While employed by all cells and tissues, AS regulation plays a particularly critical role in the mammalian brain ([26,27](#)). Indeed, high-throughput transcriptome analyses revealed that brain displays the most complex and dynamic AS network, leading to expression of neuron-specific protein isoforms ([27–29](#)). AS regulation affects all key biological processes involved in neuronal functions, such as differentiation and migration, axon guidance, synapse formation and membrane physiology. In this way, this process crucially contributes to the establishment and/or maintenance of the functional complexity of the brain ([26–27,30](#)). Transcript diversification via AS is achieved through the coordinated activity of RNA-binding proteins (RBPs), that bind pre-mRNA and alter spliceosome assembly and splice site choice ([19,31](#)). Fine-tuned modulation of the expression, localization and activity of specific RBPs orchestrates the temporal patterns of cell and tissue-specific splice variants ([20](#)). For instance, changes in expression of specific RBPs during the transition from neural progenitor cells to differentiated neurons was shown to modulate specific splicing networks that impact on key developmental processes in the brain ([32–34](#)).

In this study, we found that depletion of EWS by RNA interference promotes neuronal differentiation and neuron complexity in both neural progenitor cells (NPCs) and N2A neuron-like cells. Transcriptome analysis of EWS-depleted N2A cells identified hundreds of genes regulated by this RBP at splicing levels. Notably, splicing of several of these genes was also modulated during neuronal differentiation and EWS depletion promoted a splicing pattern similar to that of mature neurons. Furthermore, we demonstrated that EWS directly binds the pre-mRNAs of the regulated targets, including *Foxp1*, to promote splicing switches related to neuronal differentiation. These findings uncover a new role for EWS in the developmental splicing switch occurring in neuronal cells and highlights an unprecedented link between EWS, *Foxp1* and neuronal differentiation.

MATERIALS AND METHODS

Neural progenitor cells isolation and culture

Neural progenitor cells (NPCs) were isolated from C57/BL6 (Charles River Laboratories, Sulzfeld, Germany) embryonic mouse cortex at embryonic day 13.5 (E13.5), following the Institutional guidelines of the Fondazione Santa Lucia and the approval of the local Ethical Committee. After olfactory bulbs, ganglionic eminences and

meninges removal, embryonic cortices were isolated, mechanically disaggregated and centrifugated, the pellet was resuspended in neurosphere medium consisting of DMEM-F12 (1:1) with GlutaMAX™, B27 (1 ml/50 ml, Thermo Fisher Scientific), penicillin (100 U/ml), streptomycin (100 mg/ml) and supplemented with epidermal growth factor (EGF, 20 ng/ml, Peprotech, United Kingdom) basic fibroblast growth factor (bFGF, 20 ng/ml, Peprotech) and heparin (0.5 U/ml, Sigma-Aldrich). The cells were incubated in a humidified atmosphere with 6% CO_2 at 37°C. For clonal analysis, 2500 NPCs were plated in 35-mm wells. After 5 days of culture in proliferating conditions, neurosphere number was evaluated and NPC clonogenicity was calculated as ratio between plated cells and neurospheres formed, expressed as percentage. For the differentiation studies, dishes were coated with poly-ornithine (Sigma-Aldrich) in H_2O, and with laminin-1 (Sigma-Aldrich) in PBS for 1 h each at 37°C. After three washes in PBS, cells were plated in neurosphere medium containing 1% FBS and incubated in a humified atmosphere with 6% CO_2 at 37°C for 3 days.

Neural progenitor cells transfection

For transfection, NPCs were electroporated using AMAXA nucleoflector device II and AMAXA mouse NPC nucleoflector kit (Lonza, Switzerland), following manufacturer instructions. Briefly, 5×10^6 NPCs were centrifuged and resuspended in 100 μl of P3 primary solution with 300 nM of sictrl or si*Ewsr1*. Electroporated NPCs were resuspended in 500 μl of pre-warmed medium, centrifuged at 1300 rpm for 5 min at room temperature and resuspended in NPC proliferation medium.

Cell cultures and transfections

Mouse N2A cells (ATCC) and human SHSY5Y (ATCC) were maintained in Dulbecco's modified Eagle's medium (DMEM, GIBCO—Thermo Fisher Scientific, Waltham, MA, USA) with GlutaMAX™, supplemented with 10% fetal bovine serum (FBS), penicillin (100 U/ml) and streptomycin (100 mg/ml) (all from GIBCO). For differentiation studies, N2A cells were plated in DMEM with GlutaMAX™, supplemented with 0.5% FBS, penicillin (100 U/ml) and streptomycin (100 mg/ml) for 6 days. Transfection of N2A and SHSY5Y cell lines was performed using RNAimax reagent (Thermo Fisher Scientific) according to manufacturer's instructions. Briefly, 50 000 cells were subjected to double pulse of reverse-transfection by using 2 μl of Lipofectamine RNAiMAX, and cells were collected 24 h after the last pulse of transfection. N2A cells were transfected with control siRNA and siRNA for *Ewsr1* and *Foxp1* (Sigma-Aldrich, St Louis, MO, USA) at the final concentration of 25 nM. SHSY5Y cells were transfected with control siRNA and siRNA for *EWSR1* at the final concentration of 25 nM (Santa Cruz Biotechnology). siRNA sequences are reported in Supplementary Table S3.

For Antisense oligonucleotide (ASO) activity assays, transfection of N2A cell line was performed according to manufacturer's instructions. Briefly, 50,000 N2A cells were seeded in 6-well plates and transfected with ASOs at the final concentration of 5, 10 or 20 μM. Cells were collected

24h or 48h after transfection for RNA or protein extraction. ASOs were designed and synthesized by Gene Tools (Oregon, USA) to target either *Foxp1* exon 16 5′ splice site (ASO 5′SS), or EWS binding sites in the intron 16 of *Foxp1* pre-mRNA (ASO FOXP1), in the intron 7 of *Ptbp1* pre-mRNA (ASO PTBP1), in the intron 1A of *HnrnpA3* pre-mRNA, or a Standard Control Oligo (ASO ctrl). All ASOs were diluted with enzyme-free water to the final concentration of 1 mM and stored at room temperature. The sequences of ASOs are listed in Supplementary Table S3.

Immunofluorescence analysis

N2A cells were fixed for 20 min with 4% paraformaldehyde (PFA, Sigma-Aldrich) in PBS, washed in PBS three times (one fast, two for 5 min). Cells after were permeabilized with 0.2% Triton X-100 in PBS for 10 min, were incubated with 5% Bovine Serum Albumine (BSA) in PBS for 1 h at room temperature. After PBS washes, cells were incubated for 2 h with primary antibody mouse anti-β-III-tubulin (1:400, T8578, Sigma-Aldrich). Cells, after three washes in PBS, were incubated for 1 hour with Cy2-conjugated goat anti-mouse IgG (1:500, Alexa, Life Technologies). NPCs were fixed for 20 min with 4% PFA in PBS, washed in PBS three times (one fast, two for 5 min). Cells after were permeabilized with 1% BSA 0.1% Triton X-100 for 5 min and the primary antibodies were incubated for 2 hours at room temperature with mouse anti-β-III-tubulin (1:400, T8578, Sigma-Aldrich). After PBS washes, cells were incubated for 1 hour with Cy2-conjugated goat anti-mouse IgG (1:500, Alexa, Life Technologies). Cell nuclei were stained by 4′-6-diamidino-2-phenylindole (DAPI). SHSY5Y cells were fixed for 20 min with 4% paraformaldehyde (PFA, Sigma-Aldrich) in PBS, washed in PBS three times (one fast, two for 5 min). Cells after were permeabilized with 0.2% Triton X-100 in PBS for 10 min, were incubated with 5% bovine serum albumine (BSA) in PBS for 1 h at room temperature. After PBS washes, cells were incubated for 2 h with Alexa Fluor™ 594 Phalloidin (1:300, A12381, Life Technologies). Cell nuclei were stained by 4′-6-diamidino-2-phenylindole (DAPI).

Samples were then viewed and photographed by using confocal laser-scanning microscope (Zeiss, LSM700, Germany). Data are represented as percentage of positive cells/total cells (evaluated by the number of total nuclei). Neurite length was calculated with the ImageJ software, as previously described (35). Briefly, analysis was based on cell images acquired with confocal laser-scanning microscope (Zeiss, LSM700, Germany), followed by manual tracing of neurite length using neurite tracer and counter plugins in the ImageJ software. Images of three fields per well were taken and the neurite length was calculated from the base of the soma to the end of the neurite. Data were obtained from three independent experiments.

Live cell imaging using the IncuCyte neurite analysis

The IncuCyte ZOOM Live-cell imaging system (Essen Bio-Science, UK) was used to analyze neurite dynamics. Different parameters were quantified over time using an automated IncuCyte® Neurotrack software module, as detailed previously (36). N2A cells were seeded in 12-well plates at a density of 50 000/well and transfected with either ASOs, as described above. Plates were scanned every 6 h using a 10× objective. Twenty-five images per well were captured and images were analyzed for neurite length and branch points. The masks/filters adjustment for Neurotrack phase contrast image analysis was as follows: segmentation mode: texture; hole fill: 0; adjust size: −2 pixels; minimum cell width: 7 μm; neurite filtering: best; neurite sensitivity: 0.3 μm; and neurite width: 2 μm, detailed in (NeuroTrack™, 2020). The following parameters were quantified: neurite length (NL) = sum of lengths of all neurites pooled/ area of image field; neurite branch points (NBP) = total number of branch points/area of image field.

RNA extraction, gene expression and splicing assay analyses

Total RNA was isolated by using TRIzol Reagent (Thermo Fisher Scientific) according to the manufacturer's instructions. RNA was subjected to DNAse digestion (Qiagen) and the first-strand cDNA was obtained from 1 μg of RNA using random primers and M-MLV Reverse Transcriptase (Promega, Madison, WI, USA), following the manufacturer's instructions. Synthesized cDNA was used for conventional-PCR (GoTaq G2, Promega) and quantitative-PCR (SYBR Green Master Mix for Light-Cycler 480, Roche, Basel, Germany), according to manufacturer's instructions. For splicing assay experiments, conventional PCR analysis was performed after 35 cycles. The ratio between isoforms related to included and skipped exons was calculated from densitometric analysis by ImageJ software.

Primers used for qPCR and PCR analyses are listed in Supplementary Table S4. The comparative cycle threshold (ΔCt) method was used to analyze the absolute expression levels using *Tbp* and *L34* as control.

Protein extraction and western blot analyses

Proteins were extracted by using RIPA lysis buffer [(100 mM NaCl, 10 mM MgCl$_2$, 30 mM Tris–HCl pH 7.5, 10% glycerol) (Sigma-Aldrich)] supplemented with protease inhibitors [(10 mM NaF, 0.5 mM Na3VO4, 10 mM β-glycerophosphate and proteases inhibitors cocktail (Sigma-Aldrich)]. The extracts were incubated on ice for 10 min and then centrifuged for 10 min at 13 000 rpm at 4°C. Protein quantification was performed by using the Quick Start Bradford Protein Assay (Bio-Rad). The extracts were diluted in Laemmli buffer and boiled for 5 min. Extracted proteins (10–30 μg) were separated on 10% SDS-PAGE gels and transferred to polyvinyl difluoride (PVDF) membranes (Amersham, United Kingdom). Membranes were saturated with 5% non-fat dry milk in phosphate-buffered saline (PBS) containing 0.1% Tween-20 for 1 h at room temperature and incubated with the following antibodies overnight at 4 °C: mouse anti-GAPDH (1:1000, SC-32233, Santa Cruz Biotechnology Inc, Dallas, TX, USA), rabbit anti-EWS (1:1000, (18), mouse anti-β-ACTIN (1:1000, SC-47778, Santa Cruz Biotechnology Inc, Dallas, TX, USA), and rabbit anti-FOXP1 (1:1000, A-302-620A, Bethyl Laboratories Inc, Montgomery, AL, USA). Secondary anti-mouse or anti-rabbit IgGs conjugated to horseradish peroxidase (Amersham) were incubated with the membranes

for 1 hour at room temperature at a 1:5000 dilution in PBS containing 0.1% Tween-20. Immunostained bands were detected by a chemiluminescent method (Thermo Fisher Scientific). Densitometric analysis was performed by ImageJ software.

Crosslinking immunoprecipitation experiment

CLIP assays were performed as previously described (17). N2A cells were UV-irradiated once with 400 mJ/cm². Cell suspension was centrifuged at 1200 rpm for 5 min, and the pellet was incubated for 10 min on ice in lysis buffer (100 mM NaCl, 10 mM MgCl₂, 30 mM HEPES pH 7.6, 2 mM EDTA pH8, 10% glycerol, 0.5% Tryton-X100, RNase inhibitor, cocktail prtotease inhibitor (Sigma-Aldrich), 0.5 mM Naortovanadate, 1%, 10 mM β-glycerolphosphate and RNase inhibitor (Promega)). Samples were briefly sonicated and incubated with 10 μl of 1/1000 RNase I (Ambion, AM2295, Thermo Fisher Scientific) dilution and 2 μl Turbo DNase (Ambion, AM2238, Thermo Fisher Scientific) for 3 min at 37°C shaking at 1100 rpm, and then incubated on ice for 3 min. Samples were centrifuged at 13 000 rpm for 10 min at 4°C. For input RNA, 10% of extract used for immunoprecipitation was treated with Proteinase K for 1 h at 55°C and RNA was purified by standard procedure. 1 mg of extract was immunoprecipitated overnight using anti-EWS (18) antibody or purified rabbit IgGs (negative control) in the presence of protein A magnetic Dynabeads (Thermo Fisher Scientific). Immunoprecipitates were incubated overnight at 4°C under constant rotation. After stringent washes with high salt buffer (300 mM NaCl, 10 mM MgCl₂, 30 mM HEPES pH 7.6, 2 mM EDTA pH 8, 10% glycerol, 0.5% Tryton-X100) beads were equilibrated with PK buffer (100 mM Tris–HCl, pH 7.4, 50 mM NaCl, 10 mM EDTA) treated with 50 μg Proteinase K for 20 min at 37°C shaking at 1100 rpm. 7 M urea was added to the PK buffer and incubation was performed for further 20 min at 37°C and 1100 rpm. The solution was collected and phenol/CHCl3 (Ambion, 9722, Thermo Fisher Scientific) was added. After incubation for 5 min at 30°C shaking at 1100 rpm phases were separated by spinning for 5 min at 13 000 rpm at room temperature. The aqueous layer was transferred into a new tube and precipitated by addition of 0.5 μl glycoblue (Ambion, 9510, Thermo Fisher Scientific), 3 M sodium acetate pH 5.5 and 100% ethanol. After mixing, the solution containing retained RNA was precipitated overnight at –20°C. Purified RNA was used for qPCR analysis. Primers used to analyze EWS binding are listed in Supplementary Table S4.

RNA sequencing

For RNA-seq analysis, RNA from two biological replicates of control and three for si*Ewsr1* N2A cells were isolated and DNase digested using the RNAeasy Mini Kit (Qiagen) according to manufacturer's instruction. RNA sequencing and bioinformatics analysis were performed by IGA Technology services (Via Jacopo Linussio, 51, 33100, Udine, Italy).

The RNA-seq experiment was performed with 33.7 M depth of paired reads (150 bp) per sample, in three biological replicates. After the clustering analysis, one scrambled sample was discarded as outlier. The quality of the reads was assessed with the software FastQC v0.11.9 (https://www.bioinformatics.babraham.ac.uk/projects/fastqc/), then low quality portions of the reads and adapters were removed with BBDuk v38 (sourceforge.net/projects/bbmap/). The minimum length of the reads after trimming was set to 35 bp and the minimum base quality score to 25. The trimmed reads were aligned against the *Mus musculus* reference genome sequence (GRCm38, Ensembl 98) with STAR aligner v2.5.0c, (https://www.ncbi.nlm.nih.gov/pmc/articles/PMC3530905/). FeatureCountsv1.4.6-p5 (https://www.ncbi.nlm.nih.gov/pubmed/24227677) was used together with the genome annotation to calculate gene expression values as raw read counts. Normalized TMM and FPKM values were calculated with the R package edgeR (https://academic.oup.com/bioinformatics/article/26/1/139/182458). Lowly expressed genes were removed with the HTSFilter package (https://www.ncbi.nlm.nih.gov/pubmed/23821648). The differential expression analysis was performed using edgeR and only the genes with an FDR equal or lower than 0.05 were considered as Differentially Expressed Genes (DEGs).

In order to identify the number of different splicing events the software rMATS v3.2.5, (https://www.ncbi.nlm.nih.gov/pubmed/25480548) was used. A *P*-value filter of 0.05 and a delta Psi of +/-10% was used to detect significant differences in splicing events.

For DEGs, gene set enrichment analysis was performed using GSEA software (37), running a pre-ranked gene list against a library of mouse gene sets. To generate the gene list, we firstly performed a differential expression analysis. Next, the results were ordered from the most up-regulated to the most down-regulated in N2A si*Ewsr1* cells. The FDR and the enrichment score (ES) were calculated by running 1000 gene set permutations.

For DEGs and significantly different splicing events, gene ontology analysis was performed using DAVID bioinformatic tool (38) to identify the most enriched Gene Ontology (GO) categories across the down- and up-regulated events.

Bioinformatic analysis

The size of exon, size of previous exon, size of following exon, size of intron, size of previous intron, size of following intron, percentage of GC in the previous intron, percentage of GC in exon, percentage of GC in the following intron were calculated using *M. musculus* (Ensembl GRCm38) as reference genome.

For splicing feature analysis in order to calculate the following values: MaxEnt Score Acceptor, MaxEnt Score Donor, Delta MaxEnt Score Acceptor-Donor, the tool called MaxEntScan (39) was used to estimate the strength of 3′ and 5′ splice sites. 5′ splice site strength was assessed using a sequence including 3nt of the exon and 6nt of the adjacent intron (http://hollywood.mit.edu/burgelab/maxent/Xmaxentscan_scoreseq.html). 3′ splice site strength was assessed using a sequence including −20nt of the flanking intron and 3nt of the exon (http://hollywood.mit.edu/burgelab/maxent/Xmaxentscan_scoreseq_acc.html).

SVM-BPfinder (https://bitbucket.org/regulatorygenomicsupf/svm-bpfinder/src/master/) was used to estimate branchpoint and polypyrimidine tract strength and other statistics. First SVM-BPfinder was used with the following options: -s Mmus -l 500 -d 20. Scores were estimated using the sequence of introns to the 3′end of exon between 20nt and 500nt. The results were filtering according to the instructions in the official website of SVM-BPfinder (http://regulatorygenomics.upf.edu/Software/SVM_BP/). Exactly the website recommends the following:

SVM-BPfinder outputs all candidate BPs. However, many can be discarded. We recommend selecting BPs according to the following rules:

- Generally, only consider BPs with svm_score > 0
- Keep BPs close to the AGEZ (distance to 3′ss is approx. within AGEZ + 9nt), with BP-score > 0 and with svm_score > 0.
- If there is only one such BP, take that one. If there is more than one, you may keep the one with the highest svm_score if you only need one BP.
- If there are none, drop the BP_score > 0 condition and consider the BPs with svm_score > 0.

*All the above filters were applied in the final results.

Motif analysis

An analysis of enriched DNA motives was performed to identify the presence of EWS binding sites in the differential spliced regions. For that purpose, BED files with the differential splicing events were produced adding a padding of 250 bp upstream and downstream of the event's coordinates. In addition, a BED file containing all the annotated exons in the mouse genome with a padding of 250 bp was produced and used as a background. The known binding sites of EWS (17) were converted to DNA motives with Homer v4.11 (https://pubmed.ncbi.nlm.nih.gov/20513432/) and then the entire mouse genome was scanned with the Homer tool scanMotifGenomeWide.pl to find all the EWS binding sites occurrences. The coordinates of the obtained sites were intersected with the padded differential spliced events and the background to calculate the occurrence in each dataset and the proportions were compared with a Fisher Exact test.

External datasets

Neural progenitor cells (NPCs) and neurons purified from E15.5 cortical cells were downloaded from the Gene Expression Omnibus with accession GSE96950 (40). The RNA-seq data of NPCs and neurons were re-analyzed using the cut-off of $P \leq 0.05$, and threshold 1.5 for the splicing index fold change. FOXP1 KD Neural stem cells (NSCs) and their respective controls (41) were downloaded from GSE101605. The cut-off of FOXP1 KD NSCs RNA-seq data was $P \leq 0.05$.

Statistical analysis

Data are presented as mean ± SD. All tests were performed using GraphPad Prism7. $P \leq 0.05$ (*) was considered signi-

ficative. For the Venn diagram comparison, significance was assessed using the hypergeometric test in to verify whether the overlap between the two groups is not due to chance. Fisher's exact test was used for comparing count data, using a total background of 38 593 genes. The test was performed within the R environment.

RESULTS

EWS regulates self-renewal and clonogenic potential of neural progenitor cells (NPCs)

To investigate the role of EWS during neuronal differentiation, we used NPCs, which recapitulate early steps of neurogenesis *in vitro* (42). We isolated NPCs from the E13.5 cortex of wild type embryos (33) and EWS expression was silenced by electroporating the cells in the presence of siRNA oligonucleotides targeting the *Ewsr1* transcript (si*Ewsr1*; Figure 1A). Under stemness conditions, NPCs form neurospheres that rapidly grow in volume (33). Knockdown of EWS markedly affected the physiological properties of NPCs, as indicated by the reduced diameter of si*Ewsr1*-transduced neurospheres with respect to those transduced with a control (ctrl) siRNA (Figure 1B, C). Accordingly, EWS-depleted NPCs exhibited reduced clonogenic potential (Figure 1D), suggesting that high EWS expression is required to maintain stemness. In line with this hypothesis, expression of two well-known stemness markers, *Sox2* and *Nestin,* were significantly reduced in EWS-depleted NPCs, whereas *βIII-tubulin* expression, a marker of neuron differentiation, was increased (Figure 1E).

Next, we performed differentiation assays by switching NPCs to serum-containing medium for 3 days (33,42). EWS-depleted NPCs differentiated with higher efficiency than control NPCs, as assessed by the increased number of β-III Tubulin positive cells after 3 days of differentiation (Figure 1F). Moreover, EWS-depleted neurons exhibited higher complexity, as shown by the increased neurite length compared to neurons derived from control NPCs (Figure 1G). To characterize the neuron type generated prematurely in EWS-depleted cultures, we monitored the expression of GABAergic (*Gad67*), Cholinergic (*Chat*) and Glutamatergic (*vGlut1*) markers by RT-qPCR. As shown in the Supplementary Figure S1, *Ewsr1* knockdown caused a significant increase in *Gad67* expression, which is associated with GABAergic neurons representing the most abundant population in this setting. By contrast, markers of Cholinergic (*Chat*) and Glutamatergic (*vGlut1*) were not significantly affected.

EWS depletion promotes neuronal differentiation of neuroblastoma N2A cells

Our results indicate that EWS promotes NPC self-renewal proficiency and limits their entry into differentiation. To investigate the mechanism underlying the impact of EWS expression on neuronal differentiation, we employed the N2A neuroblastoma cell line. These cells efficiently differentiate into neuron-like cells, express enzymes associated with neural function and are capable of generating action potentials (43). Depletion of EWS in N2A cells (Figure 2A, B) elicited a marked change in cell morphology (Figure
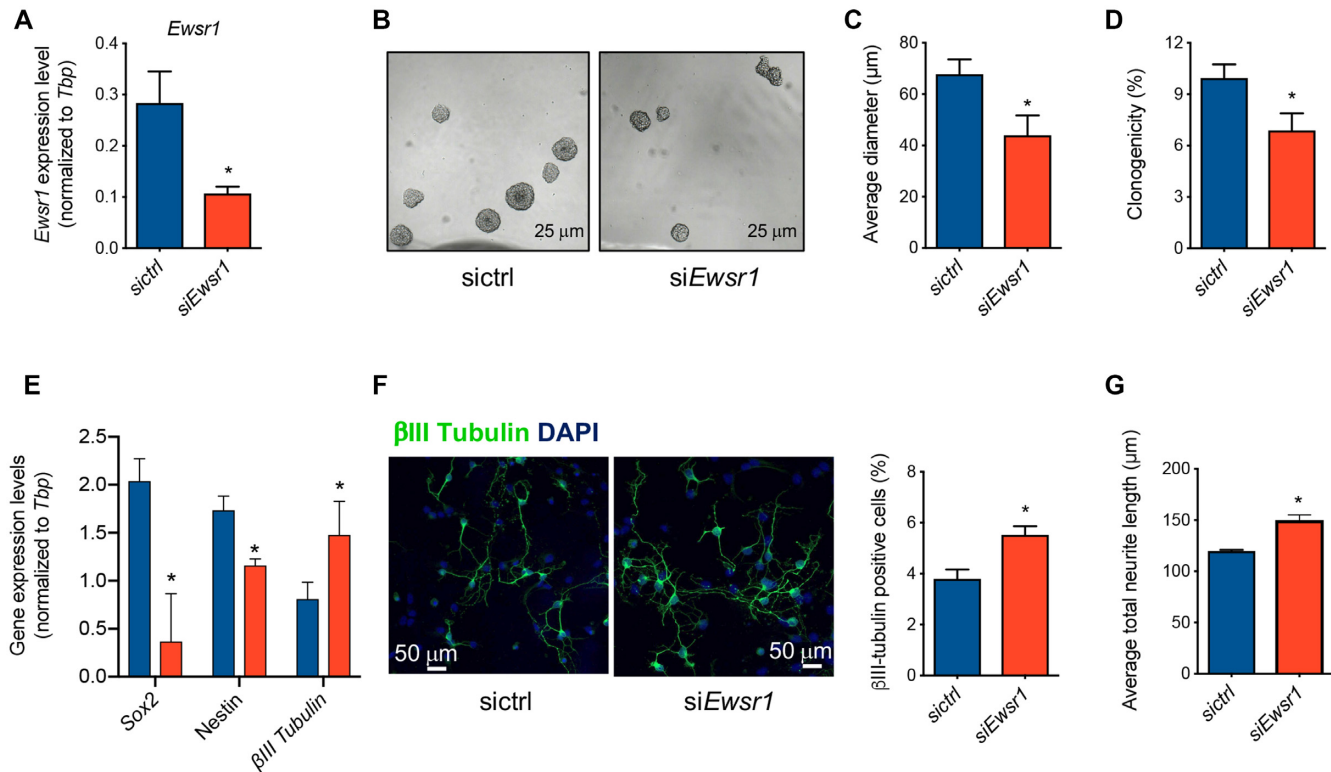
Figure 1. Knockdown of *Ewsr1* promotes neuron differentiation in Neural Progenitor Cells. (**A**). RT-qPCR showing the levels of *Ewsr1* transcript in NPCs after 48h of transfection with either sicontrol (sictrl) or si*Ewsr1*. (**B**) Representative images of NPCs transfected with sictrl or si*Ewsr1*, cultured for 5 days in proliferating condition. Scale bar = 25 μm. (**C**) Bar graph reporting the analysis of the diameter of neurospheres formed by sictrl or si*Ewsr1* NPCs after 5 days of culture. (**D**) Bar graph reporting the clonogenicity of NPCs, expressed as the percentage of neurospheres obtained from the seeded sictrl or si*Ewsr1* NPCs. (**E**) RT-qPCR showing the levels of *Sox2, Nestin* and *βIII tubulin* transcripts in NPCs transfected with either sictrl or si*Ewsr1* oligonucleotides, after 3 days of culture in differentiation conditions, normalized for the levels of the housekeeping gene *Tbp*. (**F**) Representative images of NPCs transfected with either sictrl or si*Ewsr1* oligonucleotides, after 3 days of culture in differentiation conditions. Cells were stained with anti-βIII tubulin (green), and DAPI (blue). Bar graph representing the percentage of βIII-tubulin positive cells. Scale bar = 50 μm. (**G**) Bar graph represents the average of total neurite length per cell (μm). *P*-values were determined by Student's *t* test *P ≤ 0.05 (*n* = 3; mean ± SD).

2C), with a ∼2-fold increase in the neurite length compared to control cells (Figure 2D). Similar results were also observed in human SHSY5Y neuroblastoma cells after silencing of EWS (Supplementary Figure S2A–D). Thus, EWS knockdown promotes morphological changes leading to neurite outgrowth both in human and mouse neuron-like cells.

To understand how EWS promotes morphological changes in neuronal cells, we performed RNA-sequencing (RNA-seq) analyses in N2A cells. Depletion of EWS caused extensive transcriptional changes in N2A cells (Figure 2E), with 487 genes being differentially expressed (fold change ≥ 1.5) and mostly (62%) down-regulated in *siEwsr1* cells (Figure 2F, Supplementary Table S1). Gene ontology analysis (Figure 2G) and gene set enrichment analysis (GSEA) (Supplementary Figure S1B) revealed that the EWS-regulated genes were enriched in signatures associated with chromosome organization, DNA repair, cell projection, nervous system and synaptic signaling. Notably, most of these genes were also regulated during differentiation of progenitor cells into mature neurons (40), highlighting a potential role of EWS protein in the regulation of the neuronal differentiation process. RT-qPCR analysis confirmed the expression

changes of 10 arbitrarily selected genes associated to neuronal differentiation, supporting the reliability of the RNA-seq data (Figure 2H). Collectively, these data support the hypothesis that EWS plays a key role in the switch from proliferation to neuronal differentiation.

EWS affects alternative splicing choices in N2A neuron-like cells

EWS was previously shown to regulate AS in various cell types (15–18,44). Analysis of the RNA-seq data by using the PSI-Sigma splicing patterns annotation method identified 570 AS events in 445 genes that were modulated upon EWS knockdown in N2A cells, with 350 events leading to up-regulation of the alternative region and 220 to down-regulation (Supplementary Table S2). Splicing pattern analysis showed a higher impact of EWS on exon cassette events (59%), followed by alternative 3′ splice site (19%), alternative 5′ splice site (16%), multiple-exons skipping (3%) and mutually exclusive exon (3%) events (Figure 3A). Differentially spliced genes were significantly enriched in functional categories related to RNA processing, RNA splicing and post-transcriptional regulation (Figure 3B). Analysis of
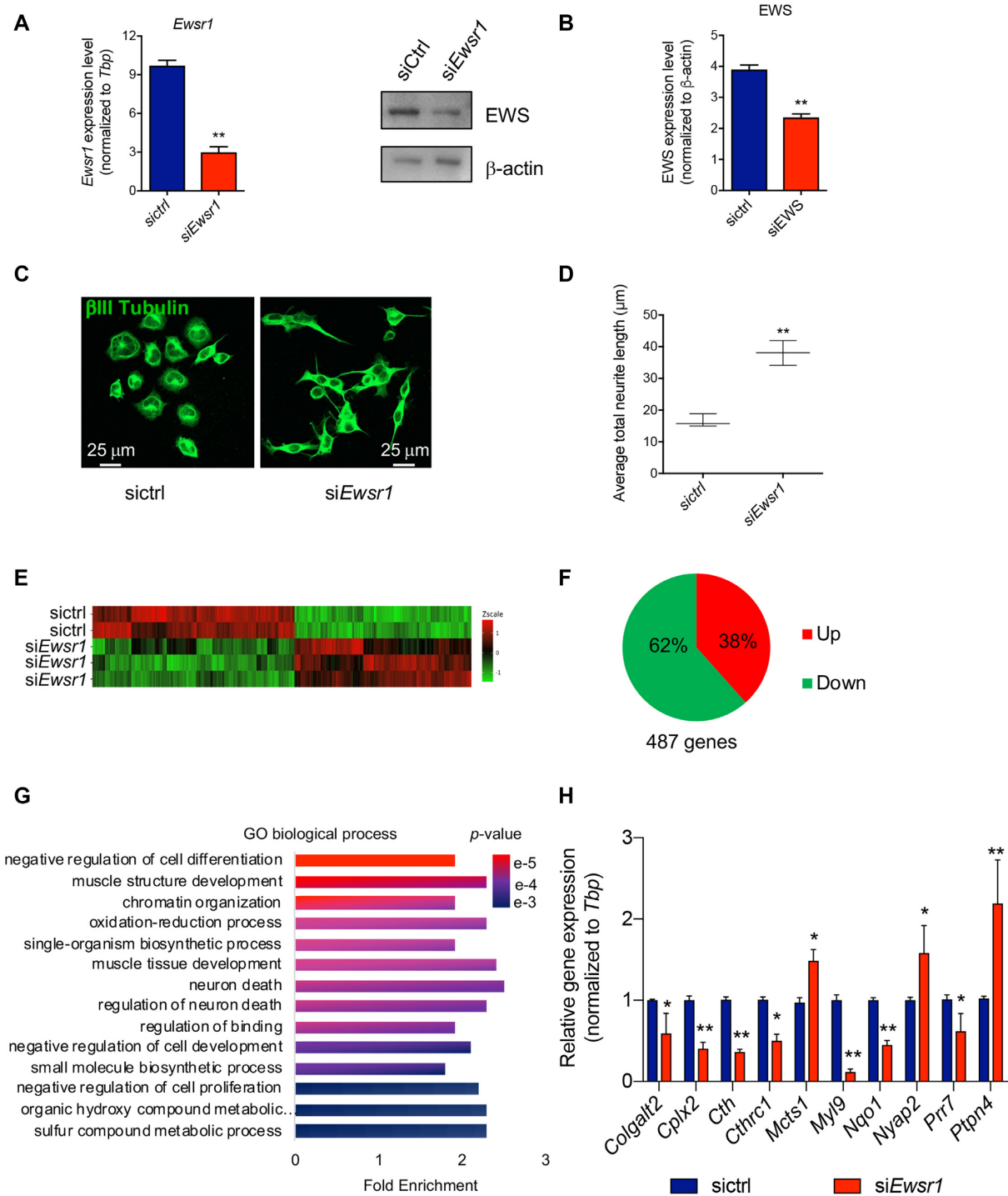
Figure 2. Knockdown of EWS promotes neuronal differentiation and leads to transcriptional changes in N2A cells. (**A**) RT-qPCR showing *Ewsr1* transcript levels in N2A cells after 48 h of transfection with either sictrl or si*Ewsr1*, normalized for the levels of the housekeeping gene *Tbp*. (**B**) Western blot showing the EWS protein levels in N2A cells after 48h of transfection with either control siRNA or si*Ewsr1*, normalized to β-actin. (**C**) Immunofluorescence analysis of N2A cells transfected with either control or si*Ewsr1* oligonucleotides for 48 h. Cells were stained with anti-βIII tubulin (green). Scale Bar = 25 μm. (**D**) Box plot showing the neurite length relative to N2A transfected with control siRNA or si*Ewsr1* for 48h. (**E**) Heatmap representing differential gene expression in control and *Ewsr1* knockdown N2A. Green color indicates down-regulated genes, and red represents up-regulated genes. Each row represents a sample and each column represents a gene. (**F**) Pie charts showing percentages of up- and down- regulated genes identified in si*Ewsr1* versus control N2A cells (fold change ≥1.5, $P \leq 0.05$). (**G**) Bar graph showing the enrichment score of the gene ontology functional clusters enriched in splicing regulated genes ($P \leq 0.01$). (**H**) RT-qPCR showing the expression levels of *Colgalt2*, *Cplx2*, *Cth*, *Cthrc1*, *Mcts1*, *Myl9*, *Nqo1*, *Nyap2*, *Prr7* and *Ptpn4* in sictrl and si*Ewsr1* N2A cells, normalized to *Tbp*. *P*-values were determined by Student's *t* test $^{*}P < 0.05$; $^{**}P < 0.01$ ($n = 3$; mean ± SD).
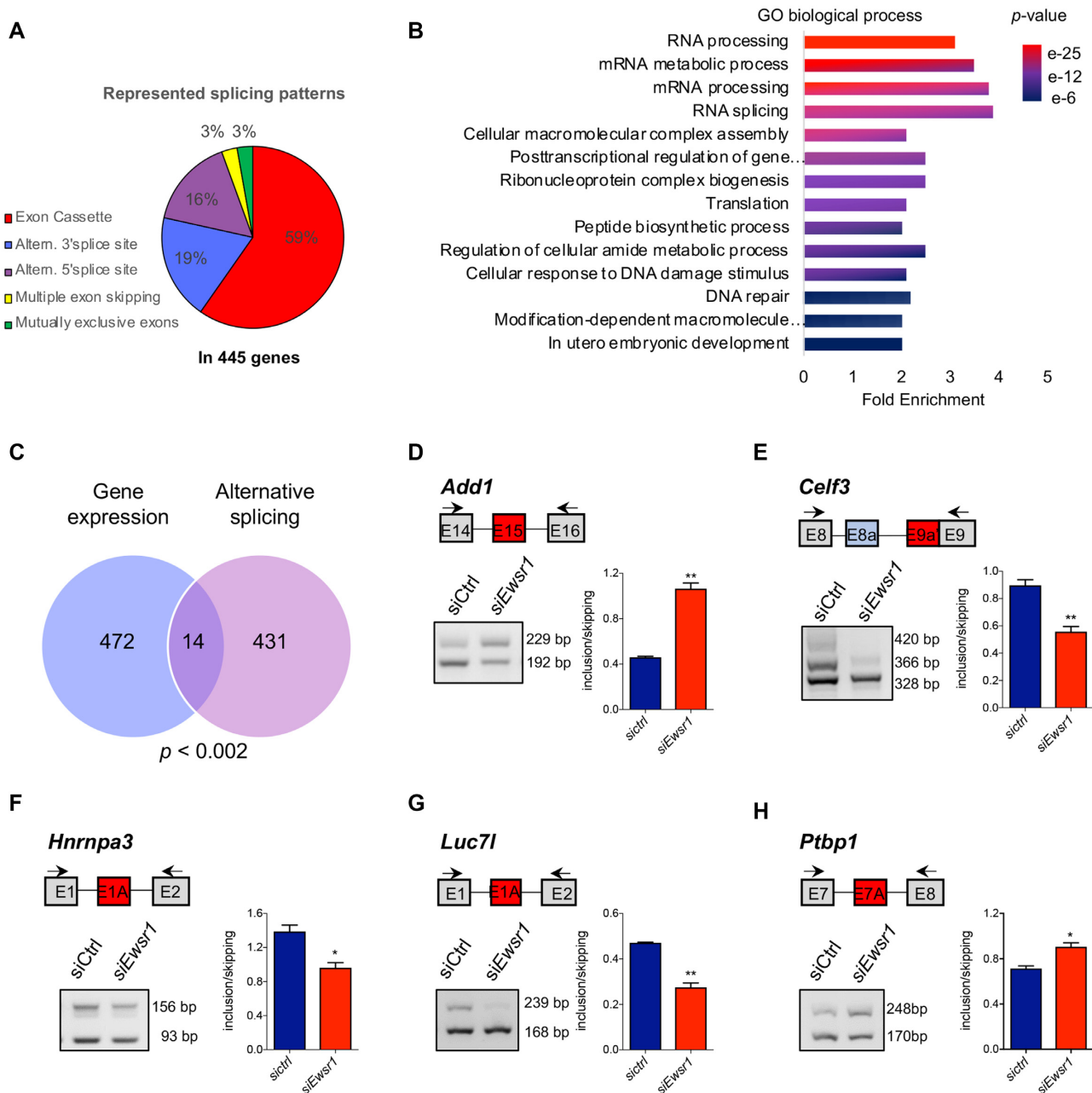
Figure 3. EWS affects alternative splicing choices of N2A cells. (**A**) Pie chart representing distribution of regulated splicing events among different splicing patterns in sictrl and si*Ewsr1* N2A cells. (**B**) Bar graph showing the enrichment score of the gene ontology functional clusters enriched in splicing regulated genes ($P \leq 0.01$). (**C**) Venn diagram showing overlap between transcriptional- and splicing- regulated genes, identified by comparison of si*Ewsr1* versus control N2A cells ($P < 0.002$). (**D–H**) Representative images of the PCR analyses for indicated alternative splicing events differentially regulated between N2A transfected with either sictrl or si*Ewsr1*. Schematic representation for each event analyzed is depicted above the representative agarose gel. Red boxes indicate the regulated exon in si*Ewsr1* compared with control N2A cells. Black arrows in the scheme indicate primers used for the PCR analysis of *Add1*, *Celf3*, *HnrnpA3*, *Luc7l* and *Ptbp1* event. The graphs show the densitometric analysis of the ratio between isoforms with included and skipped exons. *P*-values were determined by Student's *t* test: *P ≤ 0.05, **P ≤ 0.01 ($n = 3$; mean ± SD).

the overall changes in gene expression level indicated a limited overlap with splicing- regulated genes ($P < 0.002$, Figure 3C), suggesting that splicing regulation by EWS did not directly impact on expression or stability of most of its target transcripts in neuronal cells. Validation of 9 randomly selected splicing events by RT-PCR confirmed the reliability of the RNA-seq analysis (Figure 3D–H and Supplementary Figure S3).

Sequence features of EWS regulated splicing events

To gain insights into the mechanism by which EWS modulates splicing, we searched for sequence features associated with the regulated exons. EWS-regulated exons display changes in exon length in comparison with reference not-regulated exons. In particular, up-regulated exons are significantly smaller than reference or down-regulated exons

(Figure 4A). Moreover, up-regulated exons are flanked by introns that are significantly longer than reference introns (Figure 4B, C), whereas down-regulated exons are characterized by downstream introns that are longer than those of both up-regulated and reference exons (Figure 4C).

Analysis of splice sites strength indicated that exons up-regulated in EWS-depleted cells are characterized by stronger donor and acceptor sites with respect to reference exons (Figure 4D and E). Analysis of branchpoint and polypyrimidine tract sequences did not reveal significant differences between EWS-regulated events and reference exons (Supplementary Figure S4A–E), although the distance between branchpoint and acceptor was slightly higher in regulated exons compared to reference ones (Figure 4F). Likewise, EWS regulated exons did not show differences in GC content (Supplementary Figure S5A). However, up-regulated exons were characterized by flanking introns with higher GC content, whereas only the downstream intron of down-regulated exons showed this feature (Supplementary Figure S5B and C) (45). Collectively, these results suggest that EWS represses small exons containing strong donor and acceptor sites and flanked by long, GC-rich introns. Moreover, EWS plays a positive role on splicing regulation of weak exons that are followed by long introns with high GC content.

EWS exerts a positional effect on splicing regulation of target exons

Next, to determine whether EWS directly regulates these splicing events in N2A cells, we evaluated the density of EWS binding sites in its target exons. To this end, we searched for EWS consensus motifs (GGGTG, GGGGT, GGGGA pentamers) (17) in the regulated exons and flanking intronic sequences (±250 nt). Position analysis of the EWS motifs revealed a significant increase of EWS binding sites in the region upstream of up-regulated exons, and an even more pronounced in the intron downstream of down-regulated exons (Figure 5A). By contrast, EWS binding sites were significantly depleted within both up- and down-regulated exons (Figure 5A). These results suggest that EWS exerts a positional effect on target exons, with binding nearby the 5′splice site promoting inclusion and binding nearby the 3′splice site leading to skipping.

To directly evaluate whether EWS binds to its target pre-mRNAs we performed UV-cross-linked and immunoprecipitation (CLIP) experiments in N2A cells. Analysis of the *Add1, Celf3, HnrnpA3, Luc7l* and *Ptbp1* pre-mRNAs (Figure 5B–F) revealed the direct in vivo recruitment of EWS in proximity of its binding sites (indicated as black boxes in the scheme) near the regulated exons, while putative binding sites, in other regions chosen farther from the regulated exons were not bound (Figure 5B-F). Interestingly, the CLIP assays also supported its positional effect on splicing regulation. Indeed, EWS was preferentially recruited in the downstream intron of induced exons (down-regulated upon depletion), like in the *HnrnpA3, Celf3* and *Luc7l* pre-mRNAs (Figure 5B–D), whereas its binding was detected in the upstream intron of repressed exons (up-regulated upon depletion), like in the *Add1* and *Ptpb1* pre-mRNAs (Figure 5E, F). These results indicate that binding of EWS in proximity of the 5′ splice site promotes exon inclusion, presumably by recruiting U1snRNP (17), whereas its binding near the 3′splice site leads to skipping of the target exon.

To confirm that EWS controls splicing of the regulated exons by direct binding, we designed antisense oligonucleotide (ASO) to mask its binding sites in the *Ptbp1* and *Hnrnpa3* pre-mRNAs. As shown in Supplementary Figure S6, treatment with these ASOs mimicked the effects observed with EWS knockdown, with enhanced inclusion of exon 7A in *Ptbp1* and repression of the exon 1A alternative 5′ splice site in *Hnrnpa3*. These results indicate that preventing EWS binding to its target pre-mRNAs, either by protein depletion or by competition with an ASO, directly affects the splicing decision.

EWS-regulated events are modulated during neurogenesis

Developmental analysis of the mouse cortex showed that EWS protein levels peak at E15.5, whereas its expression slowly declines at birth and in early post-natal life (Figure 6A) (13). The high EWS expression at E15.5 corresponds to a stage of intense neurogenesis in the developing cortex (46,47), whereas its decline correlates with terminal differentiation of neurons (P0) and establishment of functional synaptic contacts in the cortex (P8-21) (46). Thus, we decided to compare the EWS-dependent splicing events with those differentially regulated between NPCs and post-mitotic neuronal cells in the E15.5 mouse cortex (40). Our analysis revealed a highly significant ($P = 1.67e–34$) overlap between AS events regulated in si*Ewsr1*-N2A cells and those differentially spliced upon neuron differentiation *in vivo*, with 49 events in common between the two datasets (Figure 6B). Analysis of 6 of these events showed that they were differentially modulated in the mouse cortex between E13.5, when the vast majority of cells are NPCs, and P1, when post-mitotic neurons are predominant (Figure 6C–H). Notably, these events were regulated in the same direction also during neuronal differentiation of N2A cells *in vitro*. More importantly, depletion of EWS in undifferentiated N2A recapitulated the splicing pattern that typifies N2A differentiated *in vitro* and the mouse P1 cortex with respect to the E13.5 cortex *in vivo* (Figure 6C–H). These results suggest that high EWS expression in NPCs maintains the undifferentiated splicing signature and that its depletion or physiological decline promotes the neuronal differentiation program by modulating AS choices.

EWS modulates *Foxp1* splicing during neurogenesis

Among the EWS splicing-regulated genes, we focused on *Foxp1*. The *Foxp1* gene encodes a transcription factor whose expression in NPCs promotes neuron and astrocyte differentiation (41). Importantly, FOXP1 mutations have been linked to neurodevelopmental disorders in humans (48,49), further indicating the key role played by this transcription factor in neurogenesis. Depletion of EWS in N2A promoted the inclusion of exon 16, which encodes part of the Forkhead domain required for DNA binding (Figure 7A). First, we confirmed the RNA-seq results, documenting that EWS depletion promotes the inclusion of the alternative exon 16 (Figure 7B, Supplementary Figure
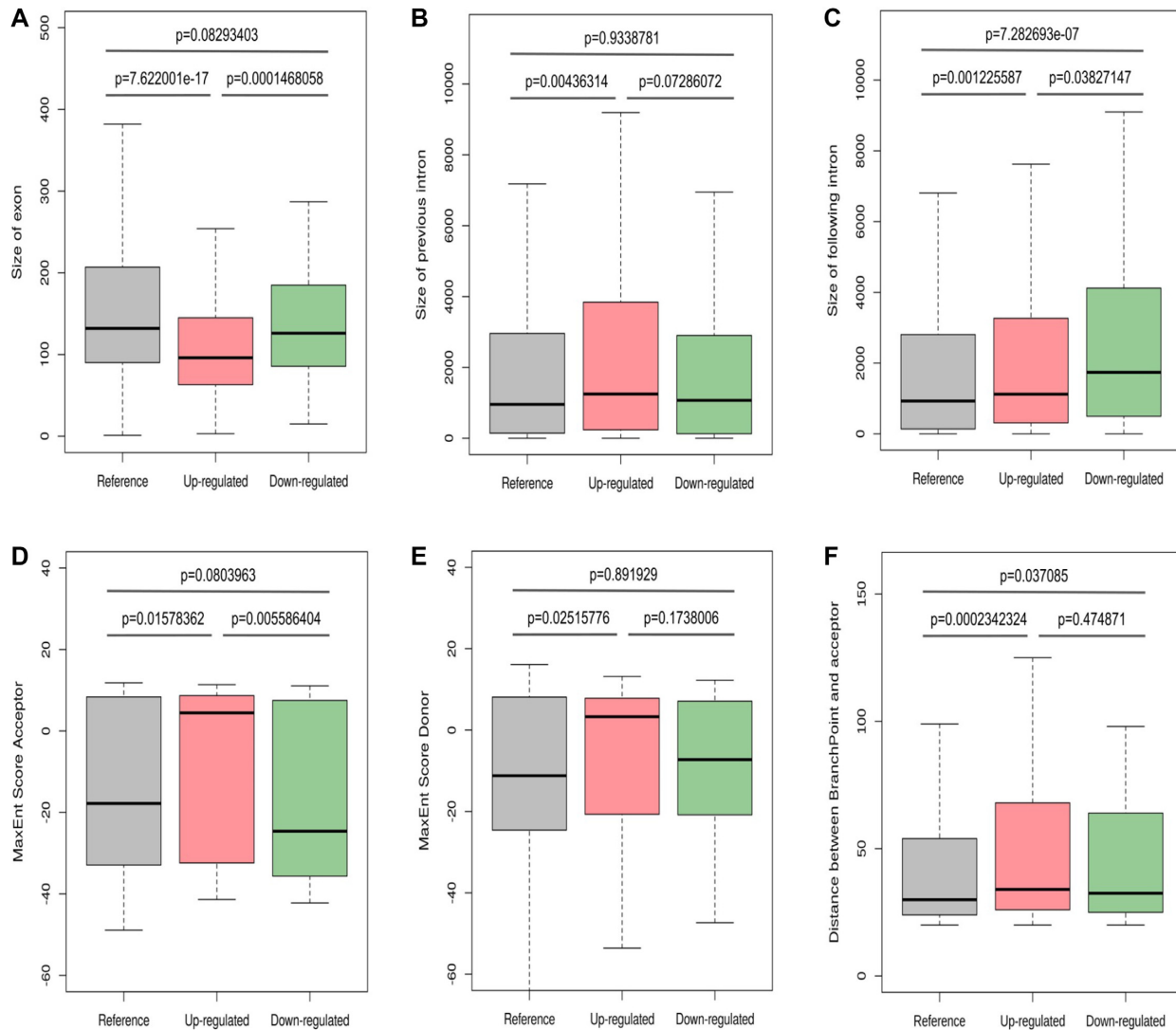
Figure 4. Sequence features of EWS regulated exons. Box plots representing comparison between up- regulated, down-regulated and reference events for exon size (**A**), previous intron size (**B**), following intron size (**C**), donor score (**D**), acceptor score (**E**), distance between branchpoint and acceptor (**F**). *P*-values are measured by Fisher test.

S7A,B), accompanied by a concomitant increase in the expression levels of the full length FOXP1 protein (Figure 7C). Importantly, increased inclusion of *Foxp1* exon 16 was also detected in the developing cortex and in NPCs depleted of EWS (Figure 7B), although with a different baseline splicing pattern compared to N2A cells. In line with a direct effect of EWS on this splicing event, CLIP experiments indicated that EWS specifically binds intronic sequences upstream of the regulated exon in N2A cells, but not in the downstream intron (Figure 7D). To corroborate the role of EWS in promoting the inclusion of *Foxp1* exon 16, we designed an ASO targeting the EWS binding motif in *Foxp1* pre-mRNA. As shown in Figure 7E, ASO treatment favored exon 16 inclusion and inhibited exon 15–17 junction, thus reproducing the effect of EWS knockdown. Moreover, blocking of EWS binding through this ASO also caused an increase in the expression of the full length FOXP1 protein (Figure 7F) and in N2A cell differentiation, monitored by

counting neurite length and neurite branch points (Supplementary Figure S8A, B).

The AS isoform promoted by EWS lacks exon 16. The 15–17 junction, which is down-regulated in EWS-depleted N2A cells (Supplementary Figure S7B), produces a frameshift and creates a premature stop codon in exon 17, which disrupts the forkhead domain. Thus, EWS could impair FOXP1 transcriptional activity by regulating splicing of exon 16. To test this possibility, we compared genes regulated by FOXP1 in NPCs cells (41) with those affected at the gene expression level upon EWS depletion in N2A cells. We observed a significant ($P < 0.001$) overlap between the two datasets, with 50 genes regulated by both EWS and FOXP1 depletion (Figure 7G). Notably, all neuronal genes in common between the two datasets were regulated in opposite direction by depletion of EWS and FOXP1, supporting the notion that EWS represses FOXP1 activity (Figure 7H). RT-qPCR analysis confirmed that a portion of
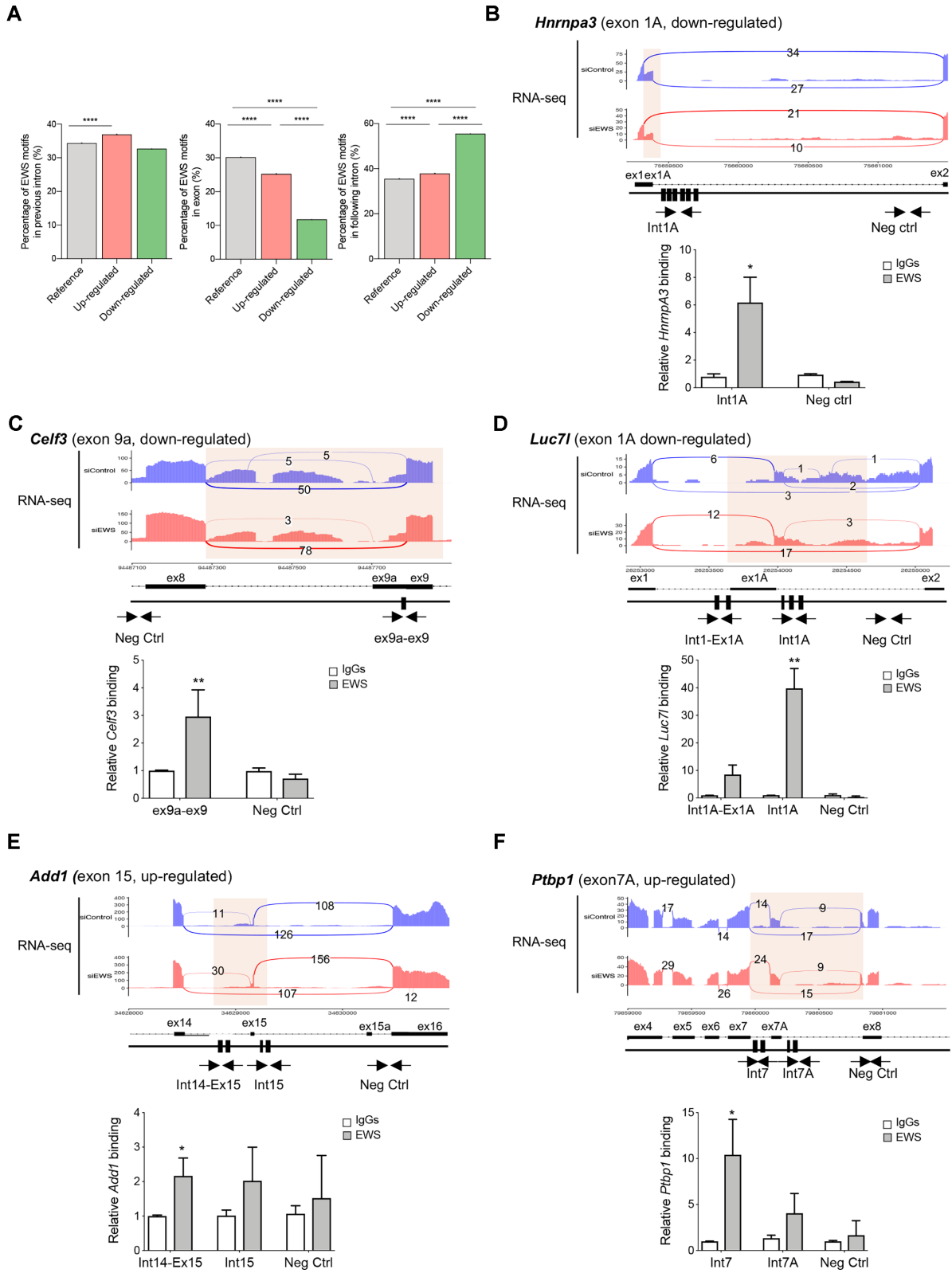
Figure 5. EWS exhibits positional pre-mRNA binding around regulated alternative splicing exons. (**A**) Bar graphs showing percentage of EWS motifs according to their relative position, 250nt at 3′ splice site, exon, 250nt at 5′ splice site, among up-regulated, down-regulated and reference exons. *P*-values are measured by Fisher exact test (****$P \leq 0.00001$). (**B–F**) Representative sashimi plots displaying RNA-Seq reads coverage of the alternatively spliced genes associated with microtubule cytoskeleton and RNA processing. Spliced regions are indicated by semi-transparent yellow blocks. Black rectangular blocks indicate EWS binding sites. Black arrows in the scheme indicate primers and amplicons used for the CLIP assay analysis. Bar graph showing qPCR signals amplified from the CLIP assays expressed as fold of IgGs. IgGs are represented in white and EWS binding in grey. *P*-value was determined by one-way ANOVA, with *P*-value <0.05, and with Bonferroni post-hoc test. *$P \leq 0.05$, **$P \leq 0.01$.
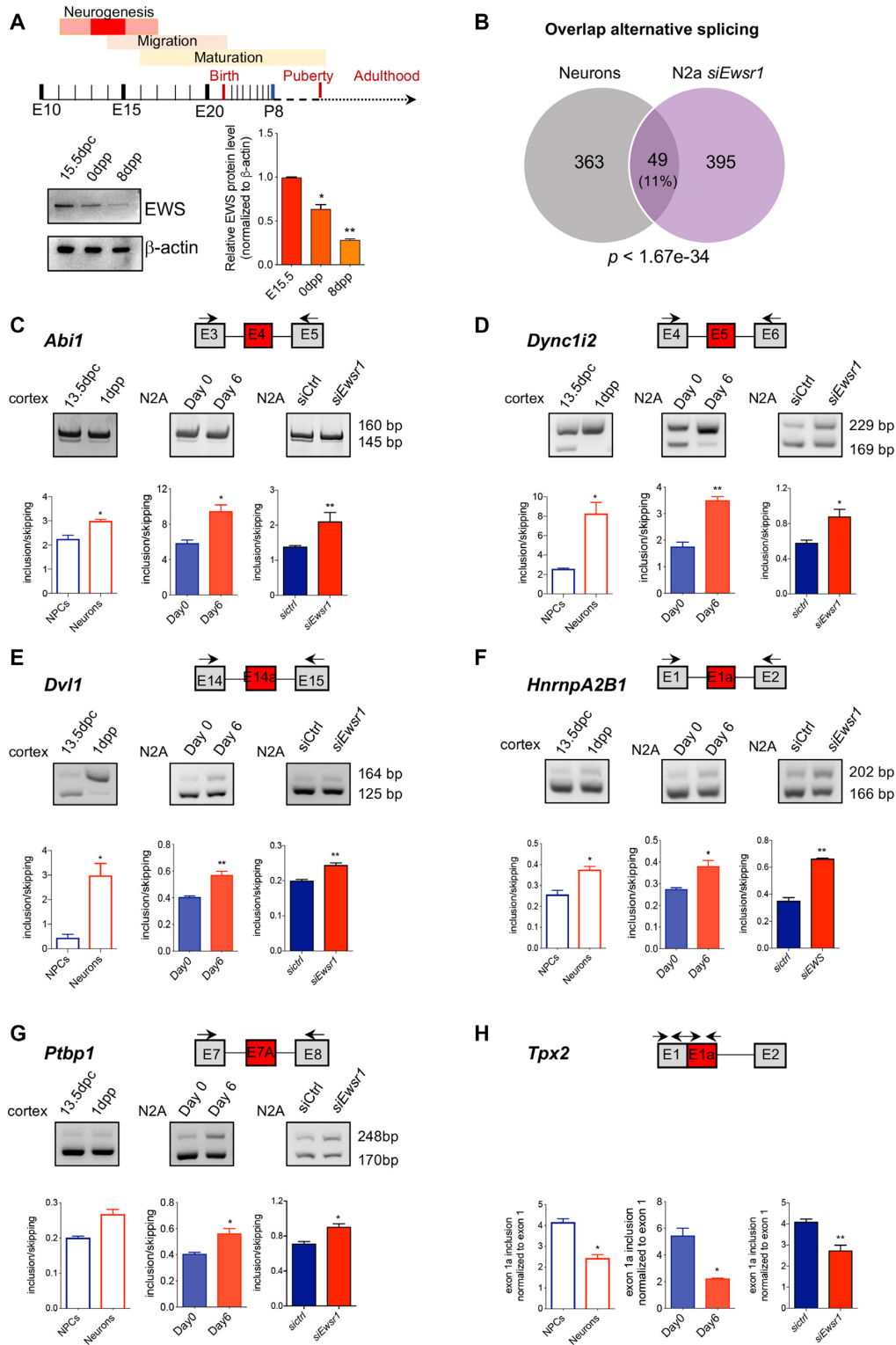
Figure 6. EWS-regulated events are modulated during neurogenesis. (**A**) Schematic representation of timing of embryonic and post-natal brain development. Western blot analysis for EWS in mouse cortex at 15.5 days post coitum (15.5 dpc), 0 day post partum (0 dpp) and 8dpp, normalized to β-actin ($n = 3$; mean ± SD). *P*-value was determined by one-way ANOVA, with *P*-value < 0.05, and with Bonferroni post-hoc test. $^*P \leq 0.05$, $^{**}P \leq 0.01$. (**B**) Venn diagram showing overlap between splicing-regulated genes, identified by comparison of si*Ewsr1*- N2A data with neuron differentiation seq- data (*P* < 1.67e–34). (**C–H**) Representative images of the PCR analyses for indicated alternative splicing events differentially regulated between N2A transfected with either sictrl or si*Ewsr1*, during neuronal development and in differentiating N2A cells. Schematic representation for each event analyzed is depicted above the representative agarose gel. Red boxes indicate the regulated exon in si*Ewsr1* compared with control N2A cells. Black arrows in the scheme indicate primers used for the PCR analysis of *Abi1*, *Dync1i2*, *Dvl1*, *HnrnpA2B1*, *Ptbp1* and *Tpx2* event. The graphs show the densitometric analysis of the ratio between isoforms with included and skipped exons. *P*-values were determined by Student's *t* test: $^*P \leq 0.05$, $^{**}P \leq 0.01$ ($n = 3$; mean ± SD).
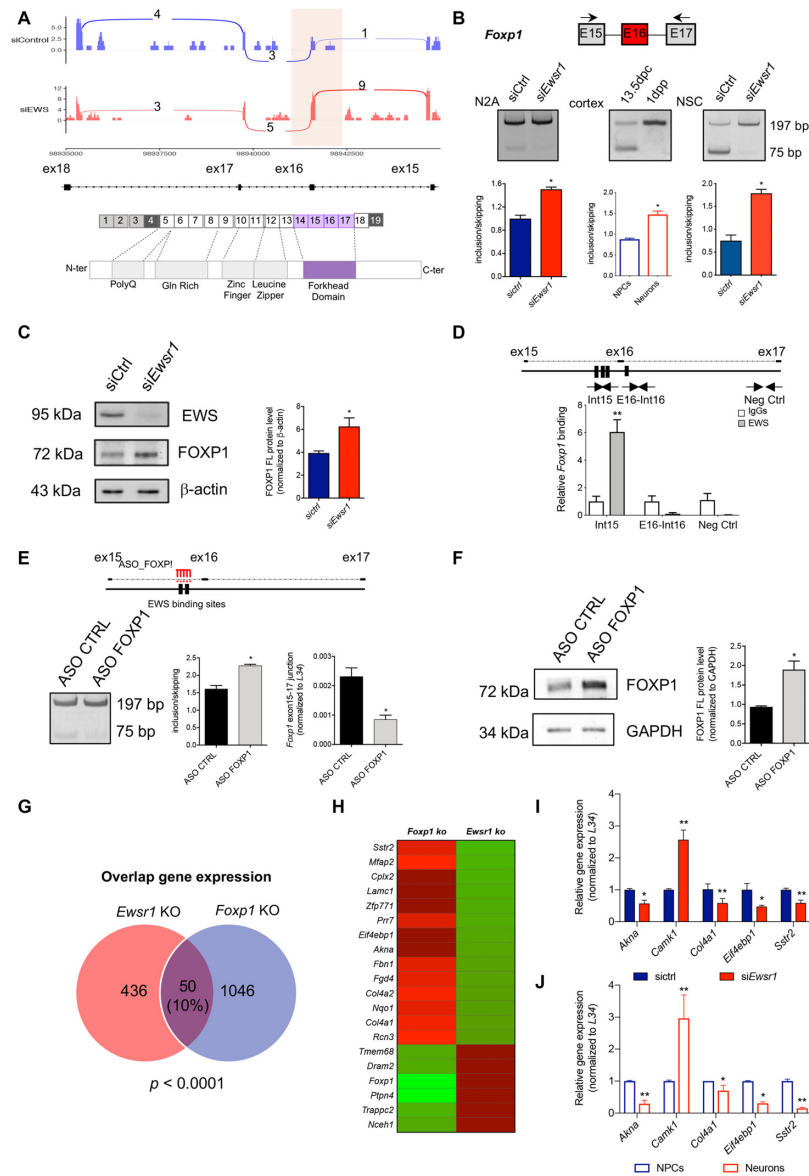
Figure 7. EWS regulates Foxp1 alternative splicing impacting neuronal gene expression. (**A**) Representative sashimi plots displaying RNA-Seq reads coverage of the alternatively spliced *Foxp1* genes. Spliced region is indicated by semitransparent yellow blocks. Schematic representation of FOXP1 protein domain. The purple exons encode for the forkhead domain. (**B**) Representative images of the PCR analyses for *Foxp1* alternative splicing event differentially regulated between N2A transfected with either sictrl or si*Ewsr1*, during cortex development and in differentiating NPCs transfected with either sictrl or si*Ewsr1*. Schematic representation for *Foxp1* event is depicted above the representative agarose gel. Red boxes indicate the regulated exon in si*Ewsr1* compared with control N2A cells. Black arrows in the scheme indicate primers used for the PCR analysis of *Foxp1* event. *P*-values were determined by Student's *t* test: $^*P \leq 0.05$, $^{**}P \leq 0.01$ ($n = 3$; mean ± SD). (**C**) Western blot analysis of sictrl and si*Ewsr1* N2A cell extracts to monitor the expression of EWS and FOXP1 proteins. Loading was normalized to β-actin expression. 15 μg of protein extracts were loaded in each lane. *P*-values were determined by Student's *t* test: $^*P \leq 0.05$, $^{**}P \leq 0.01$ ($n = 3$; mean ± SD). (**D**) Schematic representation of EWS binding sites in *Foxp1* pre-mRNA is depicted above the bar graph. Black rectangular blocks indicate EWS binding sites. Black arrows in the scheme indicate primers and amplicons used for the CLIP assay analysis. In the bottom, bar graph showing qPCR signals amplified from the CLIP assays expressed as fold of IgGs. IgGs cross-linked RNAs are represented in white, EWS cross-linked regions in grey. *P*-value was determined by one-way ANOVA, with *P*-value < 0.05, and with Bonferroni post-hoc test, $^{**}P \leq 0.01$. (**E**) Schematic representation of EWS binding sites and ASO binding in *Foxp1* pre-mRNA is depicted above the bar graph. Black rectangular blocks indicate EWS binding sites and red comb indicate ASO position used to inhibit EWS recruitment. In the bottom, representative image of the PCR analyses for *Foxp1* alternative splicing event differentially regulated between N2A treated with either ASO ctrl or ASO FOXP1. Histograms represent the densitometric analysis of the ratio between isoforms with included and skipped exons. On the right, bar graphs represent RT-qPCR analysis showing the expression levels of the junction exon 15–17 of *Foxp1* gene in N2A cells treated with ASO ctrl or ASO FOXP1, normalized to *L34*. *P*-values were determined by Student's *t* test $^*P \leq 0.05$ ($n = 3$; mean ± SD). (**F**) Western blot analysis of ASO ctrl and ASO FOXP1 N2A cell extracts to monitor the expression of FOXP1 protein. Loading was normalized to GAPDH expression. 15 μg of protein extracts were loaded in each lane. *P*-values were determined by Student's *t* test: $^*P \leq$ 0.05 ($n = 3$; mean ± SD). (**G**) Venn diagram showing overlap between transcriptional-regulated genes, identified by comparison of si*Ewsr1*-N2A data with si*Foxp1*-NSCs seq-data ($P < 0.0001$). (**H**) Heatmap representing differential gene expression in *Foxp1* and *Ewsr1* knockdown cells. Green color indicates down-regulated genes, and red represents up-regulated genes. (**I**) RT-qPCR showing the expression levels of *Akna, Camk1, Col4a1, Eif4ebp1, Sstr2* in sictrl and si*Ewsr1* N2A cells, normalized to *L34*. (**J**) RT-qPCR showing the expression levels of *Akna, Camk1, Col4a1, Eif4ebp1, Sstr2* in NPCs and neurons, normalized to *L34*. *P*-values were determined by Student's *t* test $^*P \leq 0.05$, $^{**}P \leq 0.01$ ($n = 3$; mean ± SD).

FOXP1 target genes were also modulated upon EWS depletion (Figure 7I). Moreover, these genes were also regulated during cortical development (Figure 7J), concomitantly with the opposite regulation of EWS and FOXP1 protein (Figure 8A). These results suggest that EWS controls gene expression programs associated with neurogenesis through, at least in part, splicing modulation of *Foxp1* exon 16. To directly test this hypothesis, we aimed at inducing the skipping of exon 16 in neuronal cells through an ASO that targets its 5′ splice site (ASO5'SS). Transduction of this ASO into N2A cells significantly induced skipping of exon 16 and increase in the exon 15–17 junction, as monitored by RT-PCR analysis (Figure 8B). Furthermore, the expression of this FOXP1 isoform, which is promoted by EWS, correlated with inhibition of neuronal differentiation, as determined by decreased βIII tubulin expression (Figure 8C) and reduced neurite length and branching (Figure 8D). These results confirm that EWS controls the neuronal differentiation program through, at least in part, splicing regulation of *Foxp1* (Figure 8E).

DISCUSSION

Ewsr1 knockout mice show defects in neuronal morphology, dopaminergic signaling pathways and motor function (12). However, whether EWS protein plays a direct role in these processes and though which mechanism(s) was not investigated yet. In this work, we have uncovered a new role for EWS in neuronal differentiation, which is exerted, at least part, through splicing regulation of selected target genes. Our study documents that EWS protein is strongly expressed at E15.5 in the developing cortex, which corresponds to stage of intense neurogenesis (46,47), while its expression significantly decreased at birth and in post-natal life (Figure 6A) (13). These observations suggested that downregulation of EWS protein could be required for the transition from stemness to differentiation in NPCs (50). In line with this hypothesis, depletion of EWS in NPCs isolated from wild type E13.5 cortices impaired their proliferation and clonogenic potential, reduced expression of the stemness markers *Sox2* and *Nestin*, and enhanced their tendency to differentiate into mature neurons (Figure 1). These observations indicate that high EWS expression in the developing cortex is required to maintain the pool of NPCs and to limit their premature entry into the differentiation program. Similarly, depletion of EWS in N2A cells promoted neuronal-like differentiation and increased neurite length (Figure 2C). Neurite extension is a complex process which allows neurons to achieve precise connectivity, a crucial step for their proper functioning (51). To understand the molecular mechanism underlying the morphological changes induced by EWS knockdown, we performed RNA-seq analyses in N2A cells. Most of the genes regulated upon *Ewsr1* silencing were associated with cell projection, nervous system and synaptic signaling. Notably, these functional categories were also enriched during neuronal differentiation in the developing cortex (40), supporting the role of EWS in this process.

Our analysis also identified hundreds of genes modulated at the splicing level upon EWS knockdown, with exon cassette being the predominant regulated splicing pattern (Figure 3A). Splicing-regulated genes were enriched in functional categories related to RNA processing and RNA splicing, thus supporting the strong impact of EWS on RNA metabolism in neuronal cells. Comparison between transcriptional- and splicing-regulated genes showed limited overlap (Figure 3C), indicating that EWS modulates independently transcription and splicing in neuronal cells.

Bioinformatic analysis of sequence features associated with the regulated exons revealed that EWS mainly represses small exons characterized by strong splice sites and flanked by long introns (Figure 4). In contrast, EWS promotes the inclusion of weak exons followed by long introns with high GC content. The high GC content is an important feature for the recruitment of U1 snRNP at the 5′ splice site (52). Thus, EWS could promote 5′ splice site recognition and exon definition by recruiting U1 snRNP at weak 5′ splice site, supporting previous works by our and other laboratories (15–17,44). In line with this hypothesis, position motif analysis revealed a significant enrichment of EWS binding sites near the 5′ splice site of down-regulated exons, an observation that was corroborated by CLIP experiments from UV-cross linked N2A extracts, which confirmed the direct binding of EWS to its target pre-mRNAs *in vivo*. In particular, while EWS binding nearby the 5′ splice site promotes exon inclusion, its recruitment near the 3′ splice site causes exon skipping (Figure 5), consistent with its interaction with U1 (15–17) and U2AF (17).

Alternative pre-mRNA processing plays a major role in the brain, by balancing cell growth and differentiation and by enhancing acquisition of cell identity (20,53–55). Given that EWS expression is regulated during neurogenesis and postnatal cortical development (Figure 6) (13), and that its ablation leads to early differentiation in distinct neuronal cell models (Figures 1, 2, and Supplementary Figure S2), we compared the EWS-regulated splicing events with those regulated during neurogenesis (40). We observed a significant overlap of 11% of the genes affected in both RNA-seq experiments. Genes involved in neurite branching, synapse formation and RNA processing showed similar AS patterns in EWS-depleted N2A cells and in post-mitotic neurons of the developing cortex. Among these events, we observed the inclusion of exon 1A in *HnrnpA2B1* upon silencing of *Ewsr1* in N2A cells and during neuronal differentiation, as well as the alternative inclusion of exon 7A in *Ptbp1*. Interestingly, the inclusion of the alternative exon 1A determines the production HnRNP B1 protein, rather than HnRNP A2 (56). On the other hand, inclusion of exon 7A in *Ptbp1* yields an isoform displaying altered splicing activity, thus affecting the inclusion levels of numerous exons (57). These observations suggest that EWS may coordinate a widespread splicing program in the developing cortex through direct and indirect mechanisms.

To link EWS-mediated splicing regulation with functional outcome, we focused our attention on the transcription factor FOXP1, which plays a hierarchical role in the transcription network of pluripotency. Previous studies indicated that switching of its mutually-exclusive exons 16 and 16b controls pluripotency and reprogramming of embryonic stem cells (58). In particular, the alternative inclusion of these exons changes the DNA-binding specificity of FOXP1 protein, promoting the transcription of pluripo-
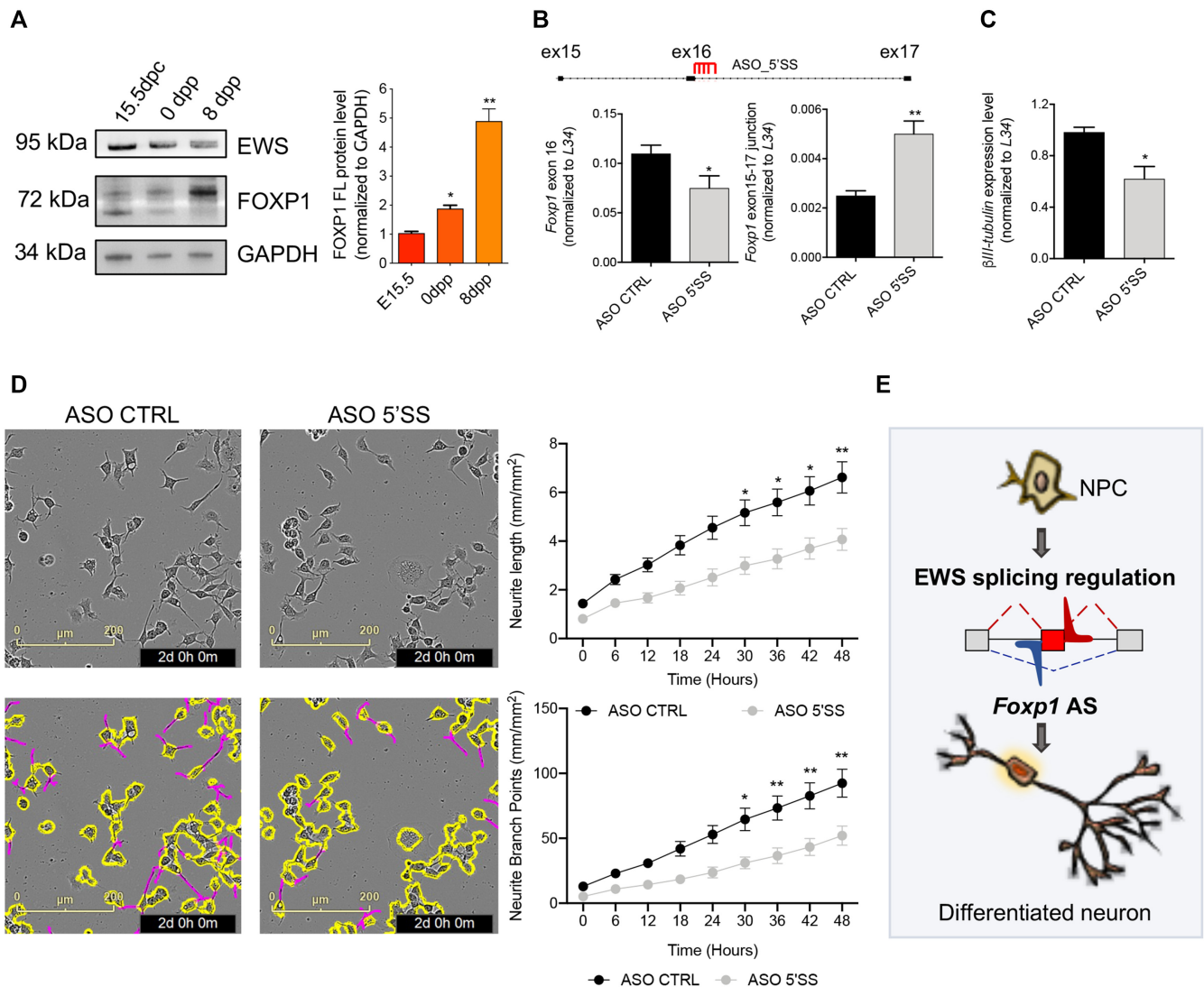
Figure 8. Foxp1 exon 16 inclusion promotes neuronal differentiation. (**A**) Western blot showing the FOXP1 protein levels in mouse cortex at 15.5 days post coitum (15.5 dpc), 0 day post partum (0dpp) and 8dpp, normalized to GAPDH ($n = 3$; mean ± SD). *P*-value was determined by one-way ANOVA, with *P*-value <0.05, and with Bonferroni post-hoc test. *$P ≤ 0.05$, **$P ≤ 0.01$. (**B**) Schematic representation of ASO 5′SS binding in *Foxp1* pre-mRNA (red comb) is depicted above the bar graph. In the bottom, RT-qPCR showing the expression levels of the exon 16 (on the left) and the *junction exon 15–17* (on the right) of *Foxp1* mRNA in N2A cells treated with ASO ctrl or ASO 5′SS, normalized to *L34*. *P*-values were determined by Student's *t* test *$P ≤ 0.05$, **$P ≤ P ≤ 0.01$ ($n = 3$; mean ± SD). (**C**) RT- qPCR showing the levels of *βIII tubulin* transcript in N2A cells treated with either ASO ctrl or ASO 5′SS for 24h, normalized for the levels of the housekeeping gene *L34*. *P*-values were determined by Student's *t* test *$P ≤ 0.05$ ($n = 3$; mean ± SD). (**D**) N2A are plated for longitudinal IncuCyte imaging and analysis of neurite length. Representative images from the IncuCyte of N2A treated with ASO ctrl or ASO 5′SS after 2 days of culture. Top row = brightfield, bottom row = overlay of cell body mask in yellow and neurite mask in pink on brightfield. Scale bars = 200 μm. Graph showing the longitudinal measurements of neurite length and neurite branch points (from 0 to 48h) relative to N2A treated with ASO ctrl or ASO 5′SS. Statistical analysis was performed by two-way ANOVA, with *P*-value <0.05, and with Bonferroni post-hoc test *$P ≤ 0.05$, **$P ≤ 0.01$ ($n = 3$; mean ± SD). (**E**) Model of the specific splicing program driven by EWS during neuronal differentiation. EWS binds intronic sequences upstream the regulated exon 16 of *Foxp1* thus promoting the skipping of exon 16. The translated FOXP1 protein can bind DNA to regulate transcription of target genes involved neuronal differentiation.

tency genes (exon 16b) or differentiation genes (exon 16) (58). Interestingly, in our experiments, we observed the inclusion of the alternative exon 16 both in N2A si*Ewsr1* cells and during *in vitro* and *in vivo* differentiation of NPCs (Figure 7A, B and Supplementary Figure S7A, B). However, exon 16b was not regulated in these different neuronal cell types and in the developing cortex. Notably, inclusion of exon 16 positively correlated with the levels of FOXP1 protein and inversely correlated with EWS expres-

sion, which decreases during neuronal differentiation (Figure 8A). *Foxp1* exon 16 encodes part of the forkhead domain, thus isoforms lacking this exon should display reduced FOXP1 activity on target genes. Accordingly, we found an inverse regulation of common neuronal gene targets upon depletion of EWS (this study) and FOXP1 (41). Moreover, an ASO that induced exon 16 skipping inhibited N2A differentiation, thus recapitulating the effects of EWS. These findings suggest that EWS contributes to regulation

of gene expression and to the timing of neuronal differentiation during neurogenesis through, at least in part, controlling the inclusion of exon 16 in the *Foxp1* pre-mRNA. Notably, *FOXP1* haploinsufficiency and heterozygous mutations in its forkhead domain have been associated with intellectual disability, autism, and language impairment (59,60). Thus, our study offers an unprecedented link between EWS splicing regulation during neuronal differentiation, *FOXP1* gene expression and neurodevelopmental disorders.

DATA AVAILABILITY

The accession number for the RNA-seq data reported in this paper is GEO: GSE173439.

SUPPLEMENTARY DATA

Supplementary Data are available at NAR Online.

ACKNOWLEDGEMENTS

FUNDING

REFERENCES

1. Tan,A.Y. and Manley,J.L. (2009) The TET family of proteins: functions and roles in disease. *J. Mol. Cell Biol.*, **1**, 82–92.
2. Bertolotti,A., Lutz,Y., Heard,D.J., Chambon,P. and Tora,L. (1996) hTAF(II)68, a novel RNA/ssDNA-binding protein with homology to the pro-oncoproteins TLS/FUS and EWS is associated with both TFIID and RNA polymerase iI. *EMBO J.*, **15**, 5022–5031.
3. Paronetto,M.P. (2013) Ewing sarcoma protein: a key player in human cancer. *Int J Cell Biol*, **2013**, 642853.
4. Delattre,O., Zucman,J., Plougastel,B., Desmaze,C., Melot,T., Peter,M., Kovar,H., Joubert,I., de Jong,P. and Rouleau,G. (1992) Gene fusion with an ETS DNA-binding domain caused by chromosome translocation in human tumours. *Nature*, **359**, 162–165.
5. Toomey,E.C., Schiffman,J.D. and Lessnick,S.L. (2010) Recent advances in the molecular pathogenesis of ewing's sarcoma. *Oncogene*, **29**, 4504–4516.
6. Kovar,H. (2011) Dr. Jekyll and mr. Hyde: the two faces of the FUS/EWS/TAF15 protein family. *Sarcoma*, **2011**, 837474.
7. Couthouis,J., Hart,M.P., Erion,R., King,O.D., Diaz,Z., Nakaya,T., Ibrahim,F., Kim,H.J., Mojsilovic-Petrovic,J., Panossian,S. *et al.* (2012) Evaluating the role of the FUS/TLS-related gene EWSR1 in amyotrophic lateral sclerosis. *Hum. Mol. Genet.*, **21**, 2899–2911.
8. Couthouis,J., Hart,M.P., Shorter,J., DeJesus-Hernandez,M., Erion,R., Oristano,R., Liu,A.X., Ramos,D., Jethava,N., Hosangadi,D. *et al.* (2011) A yeast functional screen predicts new candidate ALS disease genes. *Proc. Natl. Acad. Sci. U.S.A.*, **108**, 20881–20890.
9. Li,H., Watford,W., Li,C., Parmelee,A., Bryant,M.A., Deng,C., O'Shea,J. and Lee,S.B. (2007) Ewing sarcoma gene EWS is essential for meiosis and b lymphocyte development. *J. Clin. Invest.*, **117**, 1314–1323.
10. Park,J.H., Kang,H.J., Kang,S.I., Lee,J.E., Hur,J., Ge,K., Mueller,E., Li,H., Lee,B.C. and Lee,S.B. (2013) A multifunctional protein, EWS, is essential for early brown fat lineage determination. *Dev. Cell*, **26**, 393–404.
11. Kim,K.Y., Hwang,Y.J., Jung,M.K., Choe,J., Kim,Y., Kim,S., Lee,C.J., Ahn,H., Lee,J., Kowall,N.W. *et al.* (2014) A multifunctional protein EWS regulates the expression of drosha and microRNAs. *Cell Death Differ.*, **21**, 136–145.
12. Yoon,Y., Park,H., Kim,S., Nguyen,P.T., Hyeon,S.J., Chung,S., Im,H., Lee,J., Lee,S.B. and Ryu,H. (2018) Genetic ablation of EWS RNA binding protein 1 (EWSR1) leads to neuroanatomical changes and motor dysfunction in mice. *Exp Neurobiol*, **27**, 103–111.
13. Svetoni,F., De Paola,E., La Rosa,P., Mercatelli,N., Caporossi,D., Sette,C. and Paronetto,M.P. (2017) Post-transcriptional regulation of FUS and EWS protein expression by miR-141 during neural differentiation. *Hum. Mol. Genet.*, **26**, 2732–2746.
14. Melot,T., Dauphinot,L., Sévenet,N., Radvanyi,F. and Delattre,O. (2001) Characterization of a new brain-specific isoform of the EWS oncoprotein. *Eur. J. Biochem.*, **268**, 3483–3489.
15. Knoop,L.L. and Baker,S.J. (2001) EWS/FLI alters 5′-splice site selection. *J. Biol. Chem.*, **276**, 22317–22322.
16. Knoop,L.L. and Baker,S.J. (2000) The splicing factor U1C represses EWS/FLI-mediated transactivation. *J. Biol. Chem.*, **275**, 24865–24871.
17. Paronetto,M.P., Bernardis,I., Volpe,E., Bechara,E., Sebestyén,E., Eyras,E. and Valcárcel,J. (2014) Regulation of FAS exon definition and apoptosis by the ewing sarcoma protein. *Cell Rep.*, **7**, 1211–1226.
18. Paronetto,M.P., Minana,B. and Valcarcel,J. (2011) The ewing sarcoma protein regulates DNA damage-induced alternative splicing. *Mol. Cell*, **43**, 353–368.
19. Fu,X.D. and Ares,M. (2014) Context-dependent control of alternative splicing by RNA-binding proteins. *Nat. Rev. Genet.*, **15**, 689–701.
20. Baralle,F.E. and Giudice,J. (2017) Alternative splicing as a regulator of development and tissue identity. *Nat. Rev. Mol. Cell Biol.*, **18**, 437–451.
21. Paronetto,M.P., Passacantilli,I. and Sette,C. (2016) Alternative splicing and cell survival: from tissue homeostasis to disease. *Cell Death Differ.*, **23**, 1919–1929.
22. Barbosa-Morais,N.L., Irimia,M., Pan,Q., Xiong,H.Y., Gueroussov,S., Lee,L.J., Slobodeniuc,V., Kutter,C., Watt,S., Colak,R. *et al.* (2012) The evolutionary landscape of alternative splicing in vertebrate species. *Science*, **338**, 1587–1593.
23. Irimia,M. and Blencowe,B.J. (2012) Alternative splicing: decoding an expansive regulatory layer. *Curr. Opin. Cell Biol.*, **24**, 323–332.
24. Schreiner,D., Nguyen,T.M., Russo,G., Heber,S., Patrignani,A., Ahrné,E. and Scheiffele,P. (2014) Targeted combinatorial alternative splicing generates brain region-specific repertoires of neurexins. *Neuron*, **84**, 386–398.
25. Nilsen,T.W. and Graveley,B.R. (2010) Expansion of the eukaryotic proteome by alternative splicing. *Nature*, **463**, 457–463.
26. Furlanis,E. and Scheiffele,P. (2018) Regulation of neuronal differentiation, function, and plasticity by alternative splicing. *Annu. Rev. Cell Dev. Biol.*, **34**, 451–469.
27. Raj,B. and Blencowe,B.J. (2015) Alternative splicing in the mammalian nervous system: recent insights into mechanisms and functional roles. *Neuron*, **87**, 14–27.
28. Weyn-Vanhentenryck,S.M., Feng,H., Ustianenko,D., Duffié,R., Yan,Q., Jacko,M., Martinez,J.C., Goodwin,M., Zhang,X., Hengst,U. *et al.* (2018) Precise temporal regulation of alternative splicing during neural development. *Nat. Commun.*, **9**, 2189.
29. Naro,C., Cesari,E. and Sette,C. (2021) Splicing regulation in brain and testis: common themes for highly specialized organs. *Cell Cycle*, **20**, 480–489.

30. Vuong,C.K., Black,D.L. and Zheng,S. (2016) The neurogenetics of alternative splicing. *Nat. Rev. Neurosci.*, **17**, 265–281.

31. Lee,Y. and Rio,D.C. (2015) Mechanisms and regulation of alternative Pre-mRNA splicing. *Annu. Rev. Biochem.*, **84**, 291–323.

32. Licatalosi,D.D., Yano,M., Fak,J.J., Mele,A., Grabinski,S.E., Zhang,C. and Darnell,R.B. (2012) Ptbp2 represses adult-specific splicing to regulate the generation of neuronal precursors in the embryonic brain. *Genes Dev.*, **26**, 1626–1642.

33. La Rosa,P., Bielli,P., Compagnucci,C., Cesari,E., Volpe,E., Farioli Vecchioli,S. and Sette,C. (2016) Sam68 promotes self-renewal and glycolytic metabolism in mouse neural progenitor cells by modulating. *Elife*, **5**, e20750.

34. Gehman,L.T., Meera,P., Stoilov,P., Shiue,L., O'Brien,J.E., Meisler,M.H., Ares,M., Otis,T.S. and Black,D.L. (2012) The splicing regulator rbfox2 is required for both cerebellar development and mature motor function. *Genes Dev.*, **26**, 445–460.

35. Pemberton,K., Mersman,B. and Xu,F. (2018) Using ImageJ to Assess Neurite Outgrowth in Mammalian Cell Cultures: Research Data Quantification Exercises in Undergraduate Neuroscience Lab. *J. Undergrad. Neurosci. Educ.*, **16**, A186–A194.

36. Wurster,S., Kumaresan,P.R., Albert,N.D., Hauser,P.J., Lewis,R.E. and Kontoyiannis,D.P. (2019) Live monitoring and analysis of fungal growth, viability, and mycelial morphology using the incucyte neurotrack processing module. *mBio*, **10**, https://doi.org/10.1128/mBio.00673-19.

37. Subramanian,A., Tamayo,P., Mootha,V.K., Mukherjee,S., Ebert,B.L., Gillette,M.A., Paulovich,A., Pomeroy,S.L., Golub,T.R., Lander,E.S. *et al.* (2005) Gene set enrichment analysis: a knowledge-based approach for interpreting genome-wide expression profiles. *Proc. Natl. Acad. Sci. U.S.A.*, **102**, 15545–15550.

38. Huang,D.W., Sherman,B.T., Tan,Q., Kir,J., Liu,D., Bryant,D., Guo,Y., Stephens,R., Baseler,M.W., Lane,H.C. *et al.* (2007) DAVID bioinformatics resources: expanded annotation database and novel algorithms to better extract biology from large gene lists. *Nucleic Acids Res.*, **35**, W169–W175.

39. Yeo,G. and Burge,C.B. (2004) Maximum entropy modeling of short sequence motifs with applications to RNA splicing signals. *J. Comput. Biol.*, **11**, 377–394.

40. Liu,J., Geng,A., Wu,X., Lin,R.J. and Lu,Q. (2018) Alternative RNA splicing associated with mammalian neuronal differentiation. *Cereb. Cortex*, **28**, 2810–2816.

41. Braccioli,L., Vervoort,S.J., Adolfs,Y., Heijnen,C.J., Basak,O., Pasterkamp,R.J., Nijboer,C.H. and Coffer,P.J. (2017) FOXP1 promotes embryonic neural stem cell differentiation by repressing jagged1 expression. *Stem Cell Rep.*, **9**, 1530–1545.

42. Bertram,B., Wiese,S. and von Holst,A. (2012) High-efficiency transfection and survival rates of embryonic and adult mouse neural stem cells achieved by electroporation. *J. Neurosci. Methods*, **209**, 420–427.

43. Augusti-Tocco,G. and Sato,G. (1969) Establishment of functional clonal lines of neurons from mouse neuroblastoma. *Proc. Natl. Acad. Sci. U.S.A.*, **64**, 311–315.

44. Dutertre,M., Sanchez,G., De Cian,M.C., Barbier,J., Dardenne,E., Gratadou,L., Dujardin,G., Le Jossic-Corcos,C., Corcos,L. and Auboeuf,D. (2010) Cotranscriptional exon skipping in the genotoxic stress response. *Nat. Struct. Mol. Biol.*, **17**, 1358–1366.

45. Amit,M., Donyo,M., Hollander,D., Goren,A., Kim,E., Gelfman,S., Lev-Maor,G., Burstein,D., Schwartz,S., Postolsky,B. *et al.* (2012) Differential GC content between exons and introns establishes distinct strategies of splice-site recognition. *Cell Rep.*, **1**, 543–556.

46. Paridaen,J.T. and Huttner,W.B. (2014) Neurogenesis during development of the vertebrate central nervous system. *EMBO Rep.*, **15**, 351–364.

47. Taverna,E., Götz,M. and Huttner,W.B. (2014) The cell biology of neurogenesis: toward an understanding of the development and evolution of the neocortex. *Annu. Rev. Cell Dev. Biol.*, **30**, 465–502.

48. Co,M., Anderson,A.G. and Konopka,G. (2020) FOXP transcription factors in vertebrate brain development, function, and disorders. *Wiley Interdiscip. Rev. Dev. Biol.*, **9**, e375.

49. Estruch,S.B., Graham,S.A., Quevedo,M., Vino,A., Dekkers,D.H.W., Deriziotis,P., Sollis,E., Demmers,J., Poot,R.A. and Fisher,S.E. (2018) Proteomic analysis of FOXP proteins reveals interactions between cortical transcription factors associated with neurodevelopmental disorders. *Hum. Mol. Genet.*, **27**, 1212–1227.

50. Zhao,X. and Moore,D.L. (2018) Neural stem cells: developmental mechanisms and disease modeling. *Cell Tissue Res.*, **371**, 1–6.

51. Sierra-Fonseca,J.A., Najera,O., Martinez-Jurado,J., Walker,E.M., Varela-Ramirez,A., Khan,A.M., Miranda,M., Lamango,N.S. and Roychowdhury,S. (2014) Nerve growth factor induces neurite outgrowth of PC12 cells by promoting Gβγ-microtubule interaction. *BMC Neurosci.*, **15**, 132.

52. Lemaire,S., Fontrodona,N., Aubé,F., Claude,J.B., Polvèche,H., Modolo,L., Bourgeois,C.F., Mortreux,F. and Auboeuf,D. (2019) Characterizing the interplay between gene nucleotide composition bias and splicing. *Genome Biol.*, **20**, 259.

53. Salomonis,N., Schlieve,C.R., Pereira,L., Wahlquist,C., Colas,A., Zambon,A.C., Vranizan,K., Spindler,M.J., Pico,A.R., Cline,M.S. *et al.* (2010) Alternative splicing regulates mouse embryonic stem cell pluripotency and differentiation. *Proc. Natl. Acad. Sci. U.S.A.*, **107**, 10514–10519.

54. Yeo,G.W., Xu,X., Liang,T.Y., Muotri,A.R., Carson,C.T., Coufal,N.G. and Gage,F.H. (2007) Alternative splicing events identified in human embryonic stem cells and neural progenitors. *PLoS Comput. Biol.*, **3**, 1951–1967.

55. Suzuki,H., Osaki,K., Sano,K., Alam,A.H., Nakamura,Y., Ishigaki,Y., Kawahara,K. and Tsukahara,T. (2011) Comprehensive analysis of alternative splicing and functionality in neuronal differentiation of P19 cells. *PLoS One*, **6**, e16880.

56. Kozu,T., Henrich,B. and Schäfer,K.P. (1995) Structure and expression of the gene (HNRPA2B1) encoding the human hnRNP protein A2/B1. *Genomics*, **25**, 365–371.

57. Gueroussov,S., Gonatopoulos-Pournatzis,T., Irimia,M., Raj,B., Lin,Z.Y., Gingras,A.C. and Blencowe,B.J. (2015) An alternative splicing event amplifies evolutionary differences between vertebrates. *Science*, **349**, 868–873.

58. Gabut,M., Samavarchi-Tehrani,P., Wang,X., Slobodeniuc,V., O'Hanlon,D., Sung,H.K., Alvarez,M., Talukder,S., Pan,Q., Mazzoni,E.O. *et al.* (2011) An alternative splicing switch regulates embryonic stem cell pluripotency and reprogramming. *Cell*, **147**, 132–146.

59. Hamdan,F.F., Daoud,H., Rochefort,D., Piton,A., Gauthier,J., Langlois,M., Foomani,G., Dobrzeniecka,S., Krebs,M.O., Joober,R. *et al.* (2010) De novo mutations in FOXP1 in cases with intellectual disability, autism, and language impairment. *Am. J. Hum. Genet.*, **87**, 671–678.

60. Johnson,T.B., Mechels,K., Anderson,R.H., Cain,J.T., Sturdevant,D.A., Braddock,S., Pinz,H., Wilson,M.A., Landsverk,M., Roux,K.J. *et al.* (2018) Characterization of a recurrent missense mutation in the forkhead DNA-binding domain of FOXP1. *Sci. Rep.*, **8**, 16161.